Experimental demonstration of enhanced acoustic energy harvesting with a subwavelength metamaterial plate

Zheng Zhang, Qiuyu Li, Mourad Oudich, Yongdong Pan, Yong Li

Experimental demonstration of enhanced acoustic energy harvesting with a subwavelength metamaterial plate

Zheng Zhang,[1] Qiuyu Li,[1] Mourad Oudich,[2,3] Yongdong Pan,[1] and Yong Li[4]

[1]School of Aerospace Engineering and Applied Mechanics, Tongji University, Shanghai 200092, China

[2]Université de Lorraine, Institut Jean Lamour, CNRS UMR 7198, F-54000 Nancy, France

[3]Graduate Program in Acoustics, Penn State University, State College, PA 16801, USA

[4]Institute of Acoustics, School of Physics Science and Engineering, Tongji University, Shanghai 200092, China

Emails: ypan@tongji.edu.cn and yongli@tongji.edu.cn

In this work, we propose an acoustic energy harvesting metamaterial consisting of an array of silicone rubber pillars and a PZT patch deposited on an ultrathin aluminum plate with several holes based on locally resonant mechanism. The resonance is formed by removing four pillars, drilling a few of holes and attaching the PZT patch on the aluminum plate. The strain energy originating from an incident acoustic wave is centralized in the resonant region, and the PZT patch is used to convert the elastic strain energy into electrical power. Numerical analysis and experimental results show that the proposed millimeter-scale harvester with holes obviously improves the effect of acoustic energy harvesting while performing at the subwavelength scale for sonic low-frequency environment (less than 1150 Hz). In addition, the experimental results demonstrate that the maximum output voltage and power of the proposed acoustic energy harvesting system with 16 holes of 2 mm radius are 3 and 10 times higher than those without holes at the resonant mode for 2 Pa of incident acoustic pressure. Both the number and size of holes have a significant effect on the performance of acoustic energy harvesting. The advantages of the proposed structure are easy-to-machine and full of practicality, and it can be used in broad applications for low-frequency acoustic energy harvesting.

I. INTRODUCTION

Powered by the Internet of Things (IoT), the energy supply of wireless sensor networks (WSNs) has become crucial [1]. Up to now, batteries are still been used as a major energy source for WSNs. However, batteries are usually cumbersome, require repetitive recharging and replacements, have limited lifespans, while they cannot keep up with the miniaturization of wireless sensors which are usually placed in remote and complex environment [2]. These disadvantages limit the continuous powering of WSNs and increases coasts. Therefore, researchers and engineers have been exploring alternative energy harvesting systems that can replace batteries. Energy harvesting is defined as converting ambient energy such as thermal [3], wind [4], vibration [5], sunlight [6], etc., into useful power [7]. In more recent years, metamaterials [8, 9] with unique physical properties have been widely utilized for energy harvesting such as electromagnetic metamaterials [10, 11], mechanical metamaterials [12, 13], and thermal metamaterials [14, 15].

Sound can also act as a potential power source for energy harvesting because of its cleanness, abundancy, and ubiquity. Many researchers have proposed different thermoacoustic engines and devices for energy harvesting [16, 17]. However, due to the low energy density, sound from ambient environments commonly needs to be confined, localized and then harvested through efficient conversion media such as piezoelectric [18], electrostatic [19] and electromagnetic [20] materials. Acoustic metamaterials (AMs) [21-25] with particular capabilities can be designed to manipulate sound in ways

that are not possible in natural materials [26]. Over the past few years, many researchers have made some attempts to design different types of AMs for energy harvesting [27-32]. Recently, Qi *et al* have reported a planar AM with PZT-5H patch for energy harvesting [33]. The energy harvester was composed of an array of silicone rubber pillars periodically deposited on a homogenous aluminum plate. By removing four central pillars, a resonant defect in the AM was generated, and the strain energy originating from an incident acoustic wave of 100 dB sound pressure level (SPL) was concentrated in the defect region. Besides, the PZT-5H patch was attached to the defect region for energy harvesting. However, the height of the pillars should be increased in order to work at a lower frequency [34-36]. As the height of the pillars is increased, the load on the aluminum plate then increases and, consequently, the strain energy is decreased in the defect region, which weakens greatly the harvested energy.

In this work, we propose an acoustic energy harvesting system through introducing a new defect design to overcome the limitation from the height of the pillars. We show both numerically and experimentally that the system improves significantly the energy harvesting efficiency in a low-frequency environment. We start from similar design proposed by Qi *et al* [33] in which we have added holes surrounding the central defect in-order to lower the frequency of the defect mode and introduce a mechanical "trampoline" effect [37]. Fig. 1(a) illustrates the proposed acoustic energy harvester consisting of an array of silicone rubber pillars deposited on an aluminum plate, and a defect region is formed by removing four pillars and drilling four holes with radius r_0. The defect region can strongly confine the strain energy originated from the incident acoustic wave at the resonance frequency [38-41]. Therefore, as shown in figure 1, a circular PZT-5H patch connected to an electric circuit is used to efficiently convert the elastic strain energy into electrical power. Figure 1 sketches a supercell of the AM for energy harvesting. The geometrical parameters are set to be a = 60 mm, t = 0.4 mm, r = 3 mm, h = 10 mm and r_0 =2 mm. The parameters of silicone rubber and aluminum are listed in Table I. Besides, the radius r_1 and thickness t_1 of the PZT-5H patch are 5 mm and 0.7 mm, respectively.

Table I. Parameter values of materials in calculations

Parameters	Aluminum	Silicone rubber
Density (kg/m^3)	2700	788
Young's modulus (MPa)	70000	0.86
Poisson ratio	0.33	0.49

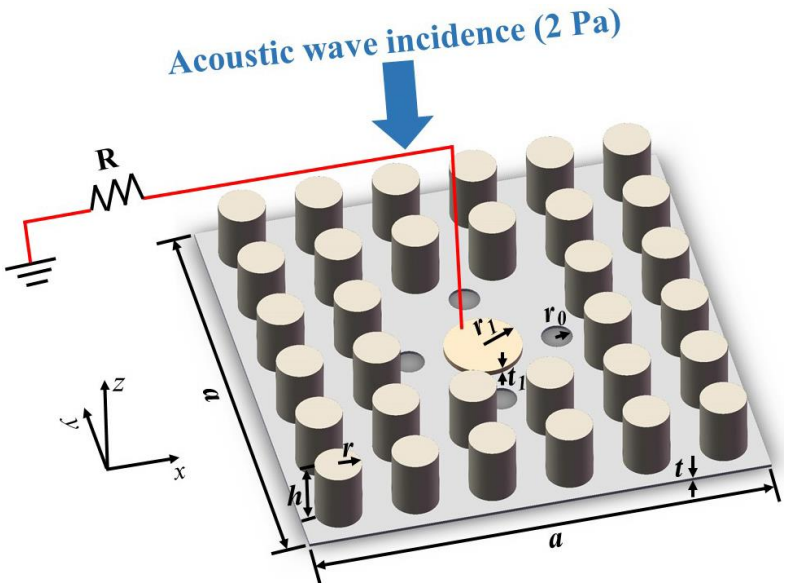

Figure 1. Schematic view of the proposed planar AM with 4 holes.

II. NUMERICAL CALCULATION AND ANALYSIS

In this study, commercial simulating software COMSOL Multiphysics Version 5.3 is used to calculate and analyze the acoustic energy harvester illustrated in figure. 1. The modules of Solid Mechanics, Pressure Acoustics, Electrostatics and Electrical Circuit are utilized to couple the acoustic, mechanical and electrostatics fields. The calculation of the band structure of the out-of-plane mode for the supercells with and without holes are shown in figures 2(a) and (b), respectively. The first irreducible Brillouin zone which is enclosed by Γ-X-M. As shown in figure 2(a), the out-of-plane band gap is obtained in the frequency range of 859-1216 Hz, which means that out-of-plane mode (the dominant modal displacement is u_z) [35, 36] are prohibited from propagation in this frequency range. Oudich *et al* has explained that only out-of-plane mode can be used to confine the sound energy [38]. Indeed, a defect mode with center frequency around 1090 Hz appears by removing four central pillars, adding the PZT-5H patch and drilling four holes in the perfect supercell, as shown in inset of figure 2(a). For the sake of comparison, the calculation of the band structure of the out-of-plane mode for the supercell without holes is shown in figure 2(b). The out-of-plane band gap is obtained in the frequency range of 857-1214 Hz, and the defect mode center frequency is around 1092 Hz. We can observe that the holes hardly change the center frequency of the defect mode. Figure 2(c) depicts the curves of sound transmission loss (STL) as a function of frequency with an incidence of 100 dB SPL. The black line represents a perfect supercell, and the yellow or blue lines correspondingly represent the energy harvesting systems with or without holes, respectively. It can be seen in figure 2(c) that STL is almost zero at the defect mode for the systems with or without holes. That is, sound energy is confined at the defect mode. Figure 2(d) describes the curves of output voltage (V) and power (P) as a function of load resistance ($R=|V|^2/2P$). The maximum output power and voltage of the proposed system with four holes (solid line) are 1.92 μW and 0.64 V, respectively. However, the system without holes (dash-dot line) can only capture the power and voltage up to 1.26 μW and 0.48 V correspondingly. When the height h of the pillars increases from 5 mm to 10 mm, the frequency of the defect band decreases from 2257.5 Hz to 1092 Hz, and the maximum output power and voltage are reduced by 86% and 63% compared to the system proposed by Qi *et al* [33]. Besides, the result shows that the system with holes can obviously improve the performance of acoustic energy harvesting in comparison with the structure without holes.

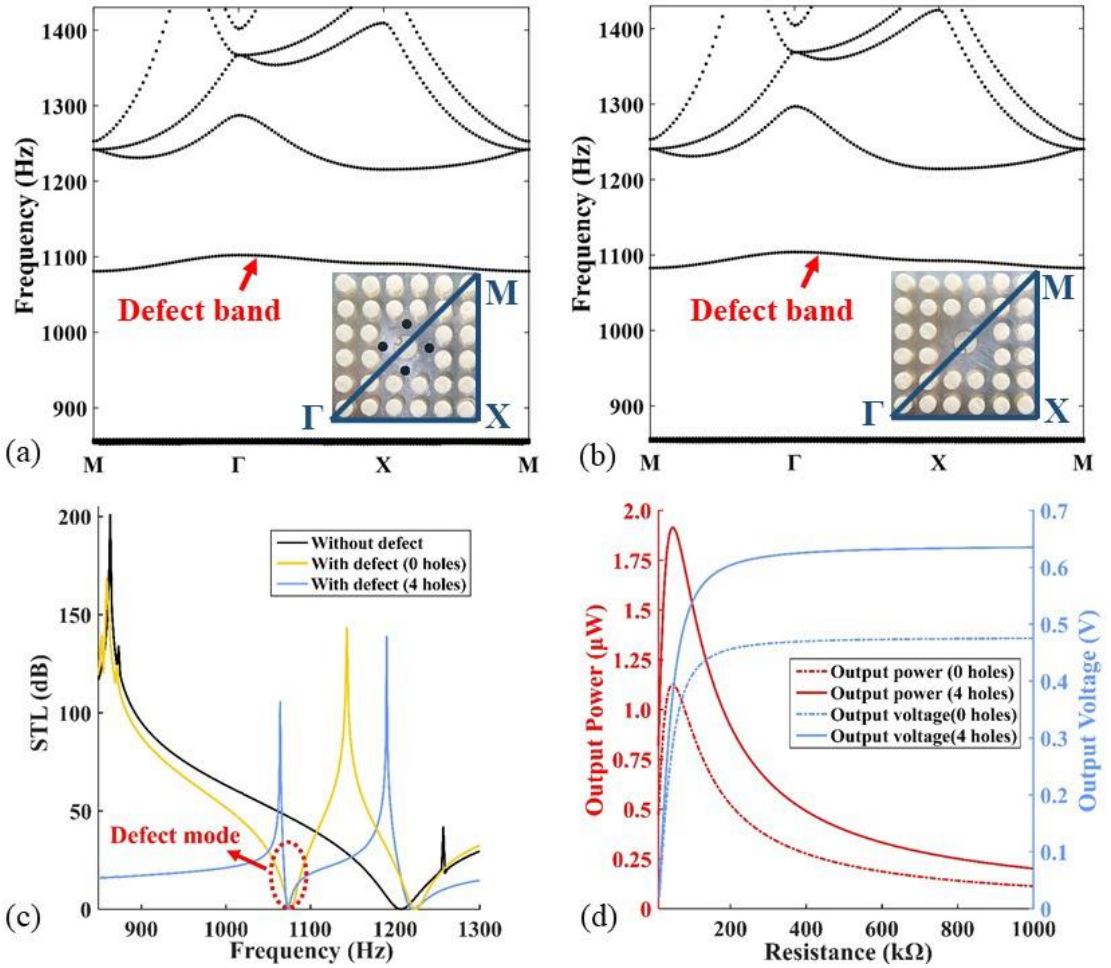

Figure. 2. Band structure of the out-of-plane mode calculated by finite element method (FEM) for the supercells with (a) or without (b) holes. The corresponding sound transmission loss (STL) versus frequency (c) and the output power and voltage versus the electrical load resistance *R* (d) at the frequency of the defect mode.

By increasing the number of holes, we further explore their effect on the performance of acoustic energy harvesting. The energy harvester with different numbers of holes described in figures 3(a)-(d). Figures 3(e) and (f) show the corresponding curves of output power and voltage as a function of load resistance for different energy harvesting systems. Both the collected maximum output power and voltage increase with the number of holes. In addition, we also investigate the performance of acoustic energy harvesting by changing the size of the holes (radius ranging from 1mm to 2mm), as shown in figures 4(a)-(c). Figures 4(d) and (e) show that both the maximum output power and voltage increase with the number of holes. The reason is that the strain energy is directly related to the output power of the PZT circuit. As shown in figures 3(e) and 4(d), the concentrated strain energy density increases with the number and size of holes, and the maximum concentrated energy density can reach up to 7 J/m^3. Therefore, the proposed millimeter-scale planar AM with holes can obviously improve the energy harvesting performance in low-frequency environment (around 1100 Hz). We have also simulated different heights of the silicone rubber pillars in order to study the influence of holes on the acoustic energy harvesting (see Appendix A for details).

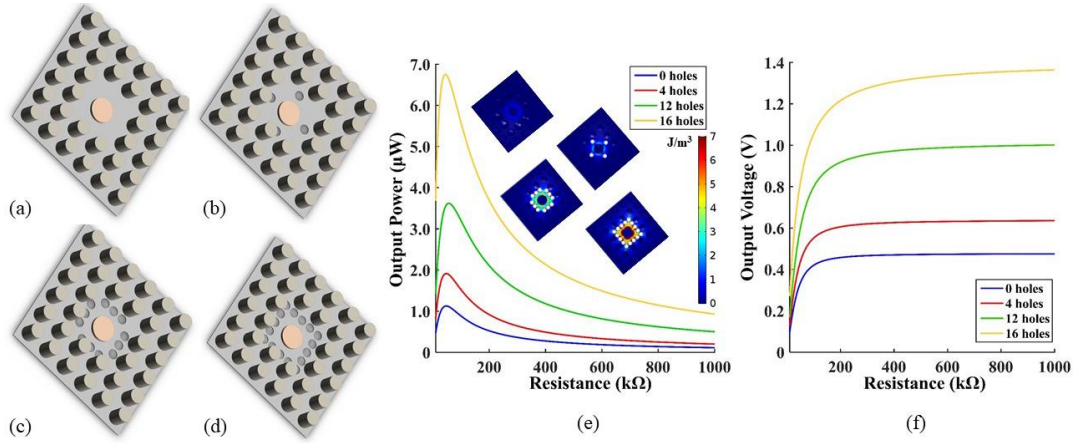

Figure 3. The planar AMs without holes (a), 4 holes (b), 12 holes (c) and 16 holes (d), and the radius of the holes is fixed to r_0 =2 mm. Output power (e) and voltage (f) versus the load resistance R at the frequency of the defect mode.

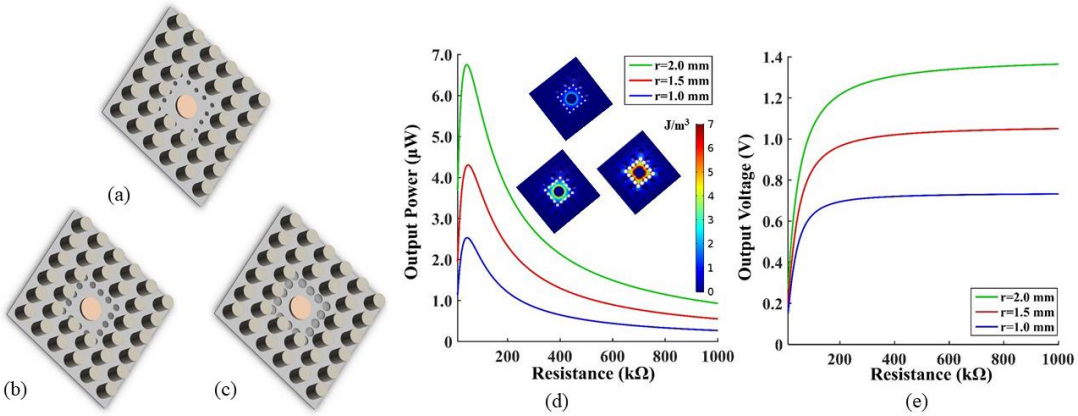

Figure 4. Different hole radius 1.0 mm (a), 1.5 mm (b) and 2.0 mm (c) for the case of planar AMs with 16 holes. Output power (d) and voltage (e) versus the load resistance R at the frequency of the defect mode.

III. EXPERIMENT DEMONSTRATION AND DISCUSSION

Regarding the experimental approach, the considered configuration described in figure 5(a) consists of 6 × 6 silicone rubber pillars deposited on a 0.4 mm thick aluminum plate. The repeated cycle of the unit cells, the height and radius of the pillars are selected to be 10 mm, 10 mm and 3.25 mm, respectively. A defect is created by removing four pillars and placing a PZT patch with 5 mm radius and 0.7mm thickness in the centeral region. Figures 5(b) and (c) illustrate the schematic representation of the experimental setup for acoustic energy harvesting and sound insulation testing separately. The experimental measurements are controlled by the personal computer (PC) with the VA-Lab IMP software module from BSWA. Under the control of the PC, sine acoustic waves are generated by the signal generator and emitted by a speaker through the audio power amplifier. The acoustic waves travel from the speaker through a rigid impedance tube (100 mm in diameter, 1480 mm in length) and then impinge on the AM along the z-direction (figure 1), as shown in figure 5(b). A microphone sensor (MPA416), Mic. 1, is used to measure the incident sound pressure, and the signals measured from Mic. 1 are sampled by the data acquisition card (MC3642) and analyzed by the PC. In addition, the PZT patch connected

with the load resistance vibrates strongly at the resonant mode, and the output voltage can be detected by the oscilloscope (Tektronix: DPO 4102B-L). Figure 5(c) shows the STL calculation in a four microphones (MPA416) impedance tube based on the transfer matrix approach. The lengths of *s* and *l* are 80 mm and 200 mm, respectively, as shown in figure 5(c). The model parameters of the experimental instruments used in figure 5(c) are the same as those illustrated in figure 5(b).

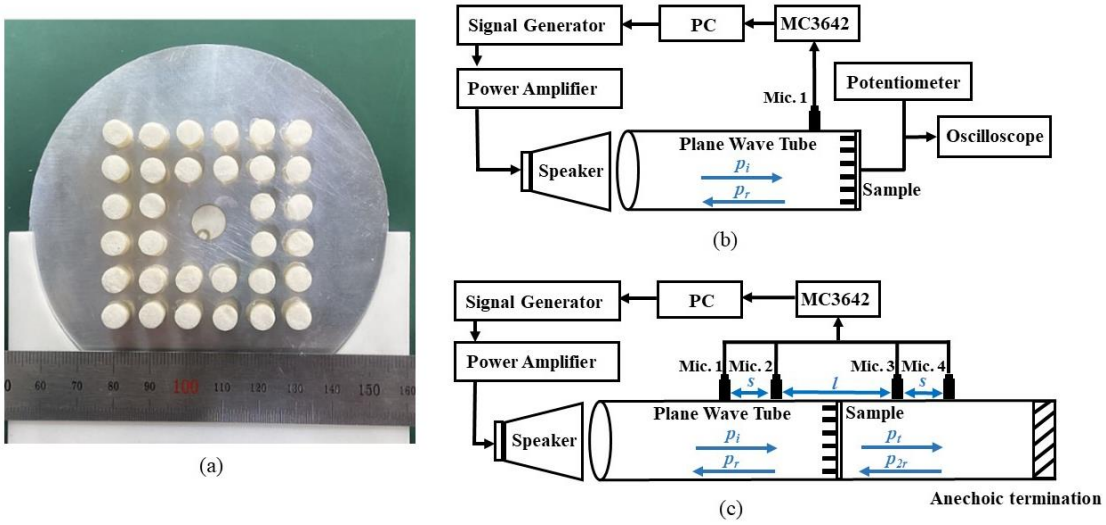

Figure 5. Experimental sample without holes (a). Schematic representation of the experimental measurement setup for acoustic energy harvesting (b) and sound insulation (c).

The microphones illustrated in figures 5(b) and (c) are used to ensure the input acoustic pressure being equal to 2 Pa (100 dB). Figure 6(a) displays numerical (red line) and experimental (blue line) STL curves of the structure shown in figure 5(a). From figure 6(a), the measured resonance frequency occurs at 1122 Hz, whereas the numerical prediction occurs at 1138 Hz. The STL trend obtained from the measurements is in good agreement with the numerical simulation. However, some unavoidable discrepancies do exist. The reasons for these discrepancies may include (but not confined) manual cutting errors of the silicone rubber pillars, surface roughness of the aluminum plate and sound leakage in the experiment. Figures 6(b) and (c) numerically (red line) and experimentally (blue markers) illustrate the output voltage and power of the planar metamaterial without holes (figure 5(a)) at the resonance frequency. From figures 6(b) and (c), the measured maximum output voltage and power are 6.64 mV and 0.065 nW, whereas the simulated maximum output voltage and power are 6.65 mV and 0.12 nW. Apart from the aforementioned reasons, the discrepancies between experiment and the simulation could be attributed to soldering tin on the PZT patch and glue among the materials. Figures 7(a) and (b) present the measured output power and voltage for the acoustic energy harvesting systems with different numbers of holes with radius r_0 =2 mm at the resonance frequency. In addition, figures 8(a) and (b) illustrate the measured power and voltage for the AM with 16 holes for different sizes of holes. Both the maximum output voltage and power increase with the number and size of holes. The trends of the experimental measurements are consistent with the predictions from the FEM calculation. The experimental results show that a maximum of 19.6 mV output voltage and 0.67 nW of electrical power can be harvested with the proposed system with 16 holes of 2 mm in radius.

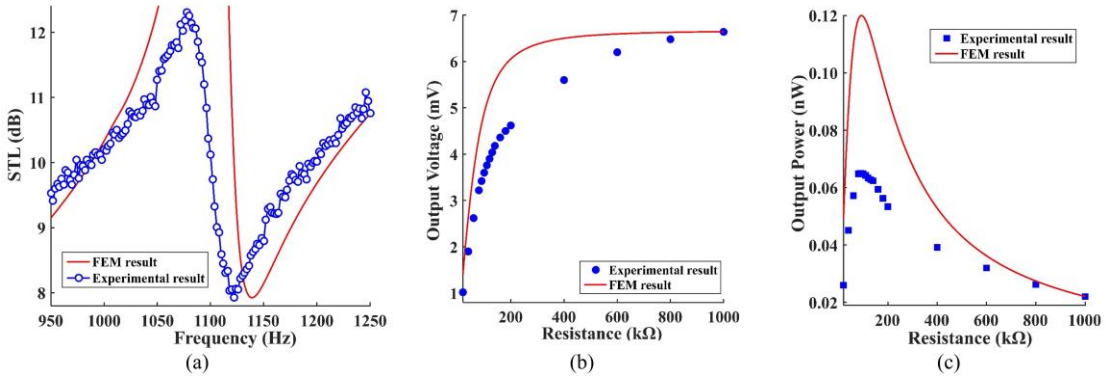

Figure 6. STL spectrum (a) of the AM without holes, and its output voltage (b) and power (c) versus the load resistance *R* at the defect mode: numerical (solid red line) and experimental (blue square dots) results.

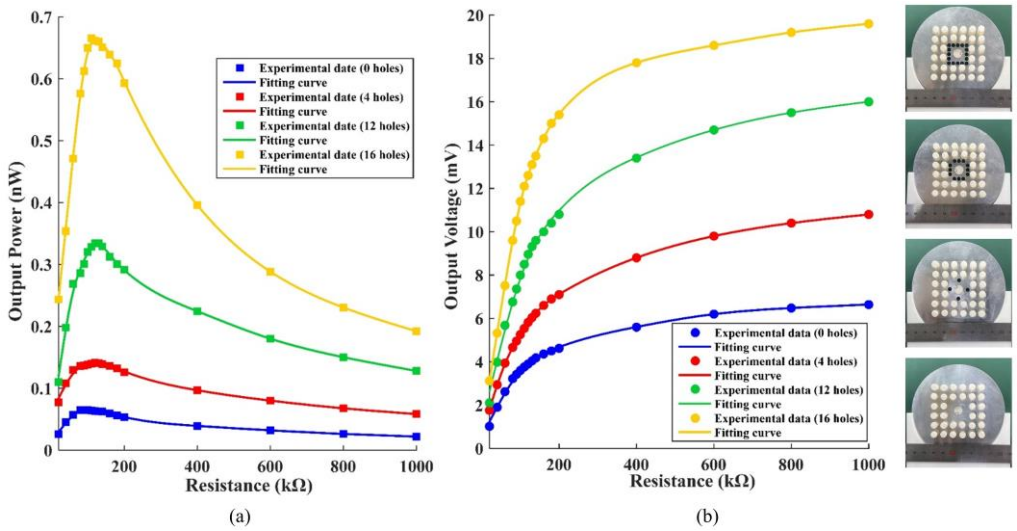

Figure 7. Output power (a) and voltage (b) versus the load resistance *R* at the frequency of the defect mode with different numbers of holes for the case of radius of 2 mm.

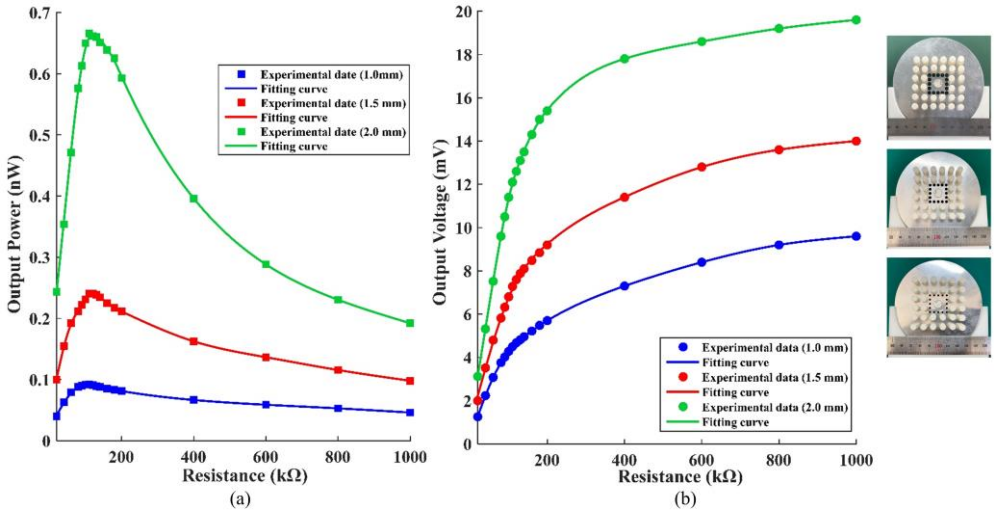

Figure 8. Output power (a) and voltage (b) versus the load resistance *R* at the frequency of the defect mode with different sizes for the structure of 16 holes.

IV. SUMMARY AND CONCLUSION

In summary, we numerically and experimentally demonstrate a millimeter-scale acoustic energy harvesting system based on a planar AM with holes. The system can significantly enhance the performance of acoustic energy harvesting. The results show that the number and size of holes will affect the output voltage and power. Both the maximum output voltage and power increase with the number and size of holes. The experimental results show that the maximum output voltage and power of the proposed system with 16 holes of 2 mm radius reach up to 19.6 mV and 0.67 nW at the resonance frequency (1122 Hz) under an incident SPL of 100 dB. These voltage and power values are about 3 and 10 times higher than those for the structure without holes. Owing to the existence of holes, the incident acoustic wave can travel through the holes and continue to propagate forward. Therefore, the demonstrated system can meet the needs of multi-frequency energy harvesting by multilayered arrangement. The system has also been proven to be an efficient, easy-to-manufacture and utility structure, and it could be widely applied in low-frequency environment.

ACKNOWLEDGMENTS

This work was supported by the National Natural Science Foundation of China (No. 11872282, 11708284) and the Young Elite Scientists Sponsorship by CAST (Grant No. 2018QNRC001).

APPENDIX A: THE INFLUENCE OF HOLES ON DIFFERENT HEIGHTS OF PILLARS

We have conducted numerical simulations on the acoustic metamaterials with different values of the pillars height h to further investigate the performance of acoustic energy harvesting by changing the number (the radius of holes is equal to 2 mm) and size (the number of holes is fixed to 16) of holes. For each value of h, the energy harvesting performance of the proposed system can be significantly improved by drilling holes in the defect region, and both the maximum output voltage and power increase with the number and size of holes, as shown in figures 9(a)-(d).

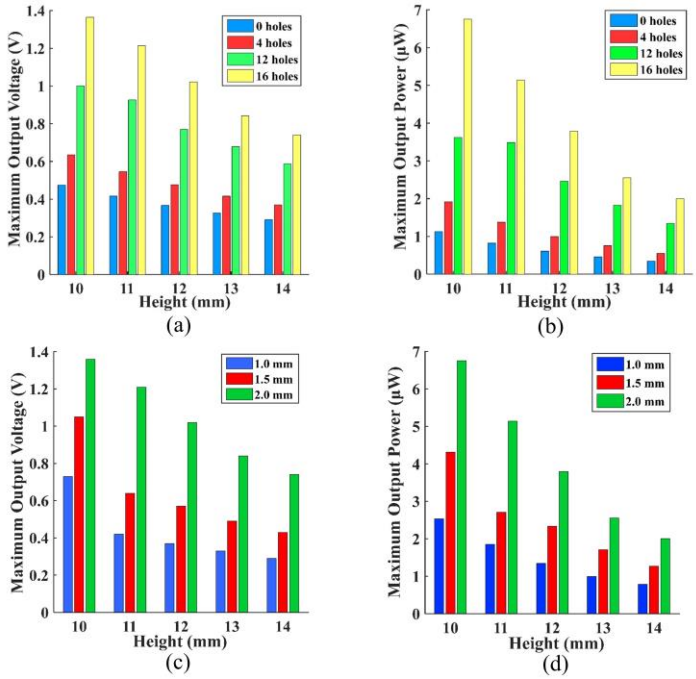

Figure 9. Maximum output voltage and power versus the height *h* of the pillars for the structures with different numbers (a), (b) and sizes (c), (d) of holes at the frequency of the defect mode.

REFERENCES

[1] Tan T, Yan Z M, Zou H X, Ma K J, Liu F R, Zhao L C, Peng Z K and Zhang W M 2019 *Appl. Energ.* **254** 113717

[2] Choi J, Jung I and Kang C Y 2019 *Nano Energy* **56** 169

[3] Donaldson L 2013 *Mater. Today* **16** 207

[4] Orrego S, Shoele K, Ruas A, Doran K, Caggiano B, Mittal R and Kang S H 2017 *Appl. Energ.* **194** 212

[5] Zhang H L, Yang Y, Su Y J, Chen J, Adams K, Lee S, Hu C G and Wang Z L 2014 *Adv. Funct. Mater.* **24** 1401

[6] Liu X R, Yuan Y F, Liu J, Liu B, Chen X, Ding J, Han X P, Deng Y D, Zhong C and Hu W B 2019 *Nat. Commun.* **10** 4767

[7] Ryu H, Yoon H J and Kim S W 2019 *Adv. Mater.* **31** 1802898

[8] Zheludev N I and Kivshar Y S 2012 *Nat. Mater.* **11** 917

[9] Della Giovampaola C and Engheta N 2014 *Nat. Mater.* **13** 1115

[10] Liu L D, Katko A R, Li D and Cummer S A 2014 *Phys. Rev. B* **89** 245132

[11] Dong Z Y, Yang F Y and Ho J S 2017 *Phys. Rev. Appl.* **8** 044026

[12] Yu X L, Zhou J, Liang H Y, Jiang Z Y and Wu L L 2018 *Prog. Mater. Sci.* **94** 114

[13] Fang H B, Chu S C A, Xia Y T and Wang K W 2018 *Adv. Mater.* **30** 1706311

[14] Li J X, Li Y, Li T L, Wang W Y, Li L Q and Qiu C W 2019 *Phys. Rev. Appl.* **11** 044021

[15] Li Y, Zhu K J, Peng Y G, Li W, Yang T Z, Xu H X, Chen H, Zhu X F, Fan S H and Qiu C W 2019 *Nat. Mater.* **18** 48-+

[16] Smoker J, Nouh M, Aldraihem O and Baz A 2012 *J. Appl. Phys.* **111** 104901

[17] Zhao D, Ji C Z, Li S H and Li J W 2014 *Energy* **65** 517

[18] Yeo H G, Ma X K, Rahn C and Trolier-McKinstry S 2016 *Adv. Funct. Mater.* **26** 5940

[19] Lin Z H, Cheng G, Lee S, Pradel K C and Wang Z L 2014 *Adv. Mater.* **26** 4690-+

[20] Costanzo A, Dionigi M, Masotti D, Mongiardo M, Monti G, Tarricone L and Sorrentino R 2014 *P. IEEE* **102** 1692

[21] Liu Z Y, Zhang X X, Mao Y W, Zhu Y Y, Yang Z Y, Chan C T and Sheng P 2000 *Science* **289** 1734

[22] Bai L, Song G Y, Jiang W X, Cheng Q and Cui T J 2019 *Appl. Phys. Lett.* **115** 231902

[23] Bai L, Dong H Y, Song G Y, Cheng Q, Huang B, Jiang W X and Cui T J 2018 *Adv. Mater. Technol-US.* **3** 1800064

[24] Li Y, Jiang X, Liang B, Cheng J C and Zhang L K 2015 *Phys. Rev. Appl.* **4** 024003

[25] Li Y, Qi S and Assouar M B 2016 *New. J. Phys.* **18** 043024

[26] Cummer S A, Christensen J and Alu A 2016 *Nat. Rev. Mater.* **1** 16001

[27] Li Y, Jiang X, Li R Q, Liang B, Zou X Y, Yin L L and Cheng J C 2014 *Phys. Rev. Appl.* **2** 064002

[28] Qi S B, Li Y and Assouar B 2017 *Phys. Rev. Appl.* **7** 054006

[29] Qi S B and Assouar B 2017 *Appl. Phys. Lett.* **111** 243506

[30] Wang X L, Xu J J, Ding J J, Zhao C Y and Huang Z Y 2019 *Smart Mater. Struct.* **28** 025035

[31] Liu G S, Peng Y Y, Liu M H, Zou X Y and Cheng J C 2018 *Appl. Phys. Lett.* **113** 153503

[32] Sun K H, Kim J E, Kim J and Song K 2017 *Smart Mater. Struct.* **26** 075011

[33] Qi S B, Oudich M, Li Y and Assouar B 2016 *Appl. Phys. Lett.* **108** 263501

[34] Assouar M B and Oudich M 2012 *Appl. Phys. Lett.* **100** 123506
[35] Oudich M, Li Y, Assouar B M and Hou Z L 2010 *New. J. Phys.* **12** 083049
[36] Pennec Y, Djafari-Rouhani B, Larabi H, Vasseur J O and Hladky-Hennion A C 2008 *Phys. Rev. B* **78** 104105
[37] Bilal O R and Hussein M I 2013 *Appl. Phys. Lett.* **103** 111901
[38] Oudich M, Assouar M B and Hou Z L 2010 *Appl. Phys. Lett.* **97** 193503
[39] Lv H Y, Tian X Y, Wang M Y and Li D C 2013 *Appl. Phys. Lett.* **102** 034103
[40] Yang A C, Li P, Wen Y M, Lu C J, Peng X, Zhang J T and He W 2014 *Appl. Phys. Lett.* **104** 151904
[41] Jiang W L, Feng D, Xu D H, Xiong B and Wang Y L 2016 *Appl. Phys. Lett.* **109** 161102